

## Alternative Method of Nature Inspired Geometrical Design Strategy for Drag Induced Wind Turbine Blade Morphology

S.N. Ashwindran, A.A. Azizuddin\*, A.N. Oumer and M.S. Idris

Faculty of Mechanical and Automotive Engineering Technology, Universiti Malaysia Pahang, 26600 Pahang, Malaysia

**ABSTRACT** – Although drag driven wind turbine is regarded as an efficient rotor for low wind speed regions, design reconfiguration is a continuous process in order to improve the performance of the rotor. The main governing factor that influences the performance of the rotor is the blade morphology. Hence, this paper presents a proposed nature-inspired design approach for the development of drag-driven wind turbine blade morphology. The design approach framework comprises three main elements, namely image processing, geometrical analysis and bio-hybridization. The proposed bio-hybridized design consists of a blade mainframe curve inspired by nautilus shell and barnacle on the blade surface. It is found that integration of barnacle geometries on the surface of the blade has affected the performance of the rotor. Result shows that the peak  $C_m$  is at  $\lambda = 0.55$  for experimental and CFD is  $C_m = 0.238$  and  $C_m = 0.253$  respectively. The proposed design resulted in experimental and numerical  $C_p = 0.113$  and  $C_p = 0.127$  respectively at 7 m/s and  $\lambda = 0.7$ . The presented design technique with appropriate design bio-element provides a systematic method for engineers to model wind turbine blade morphologies.

### ARTICLE HISTORY

Received: 15<sup>th</sup> Nov. 2021

Revised: 13<sup>th</sup> June 2022

Accepted: 22<sup>nd</sup> June 2022

Published: 28<sup>th</sup> June 2022

### KEYWORDS

*Wind turbine;*

*Savonius;*

*Bioinspiration;*

*Wind energy;*

*OpenCV*

## INTRODUCTION

Biomimicry is an approach of adapting elements from nature such as patterns, morphologies and mechanisms in order to provide a sustainable solution to the challenges faced by humans [1]. Researchers classify bio-adaptation studies into two types that are biomimicry and biomimetics. Although there is no distinct difference between the types, generally biomimicry refers to developing design and the biomimetics approach is applied for the development of military technology [2]. In 1997 Jenine Benyus published a book called “biomimicry innovation inspired by nature”, which introduced the concept and theoretical framework to biomimicry [3]. Jenine Benyus stated that nature should be referred to as “model, measure and mentor”. Furthermore, biomimicry is an innovative approach to attain sustainable designs by adapting elements from nature as nature has been evolving for the past 3.8 billion years into a feasible and perfect mechanism [4].

In this study conventional drag-driven Savonius wind turbine (SWT) configuration is adapted as a design principle. This paper presents the method on the geometrical design strategies utilized for the development of nature-inspired drag-driven WT blade. The geometrical design strategy framework consists of 3 elements, namely image processing of bio-elements, mathematical analysis of fundamental geometries and bio-hybridization of WT. A rudimentary CFD investigation is carried out to examine the performance of the WT model derived from the suggested technique. The purpose of the CFD analysis is to verify the validity of the modelling strategy utilized for the morphological design execution of the WT blade and to study the flow field behaviour and aerodynamics response of the proposed blade morphology.

## RELATED WORK

However, regions of South East Asia onshore sites have low wind speed potential, in which conventional wind power turbines can't produce sufficient power [5]. Hence, design improvement and adaptation are being implemented with the motive of obtaining a more efficient and reliable wind power device for low wind speed regions. A researcher has proposed several innovative approaches to design optimization, such as surrogate modelling, parametric-based optimization, specialized modified algorithm-based optimization, design adaptation and implementation and others. Based on all the novel approaches proposed by engineers and researchers on specialized WT, it might take years for the proposed design or mechanism to be considered feasible for commercial use [6]. The wind turbine is an electromechanical energy harvester device by means of converting the motion of wind into mechanical energy of rotation resulting in generation of electricity. The magnitude of power output depends on the intensity of the kinetic energy possessed by the wind. The introductory classification of WTs is according to its configuration relative to its axis of rotation namely vertical and horizontal axis [7]. Figure 1 illustrates the axis of rotation and configuration of WT. Generally, the hub WT is located in the atmospheric boundary layer (ABL), which is approximately at 100 m height from the ground [8]. Aside from the axis of rotation, WTs are also categorized in terms of aerodynamic dominance, that is drag and lift [9]. The aerodynamic forces or coefficients indicate the aerodynamics flow field response of the blade relative to wind load. In simple terms,

the factor that dictates the magnitude or dominance of aerodynamic forces is the blade morphology. The geometry of the turbine blade influences the flow behaviour resulting by the change in flow field properties such as pressure, rate of change of transport phenomena and velocity.

### Bioinspiration Techniques and Approaches

Design procedure in biomimicry is classified into two types of process which is top-down approach and bottom-up approach [10]. The top-down procedure is solving problems by adapting or referring to how a living organism or a particular ecosystem renders the issue as in design looking to biology. Meanwhile, the bottom-up procedure is analyzing particular traits of a living organism or ecosystem and translating them into a functional design, as in biology into design [11]. Figure 1 shows the procedure on top-bottom and bottom-up mechanisms. Application to design problem by biomimicry has three levels, namely organism level, behaviour level and ecosystem level. At the organism level, the mimicking procedure refers to adapting a particular organism's mechanism. Behaviour level is mimicking the behaviour of an organism. Where else, the ecosystem level refers to adapting to the whole mechanism of an ecosystem. There are five elements in biomimicry, namely function, material, form, process and construction [11]. The degree of adaptation is dependent on the level of elements included.

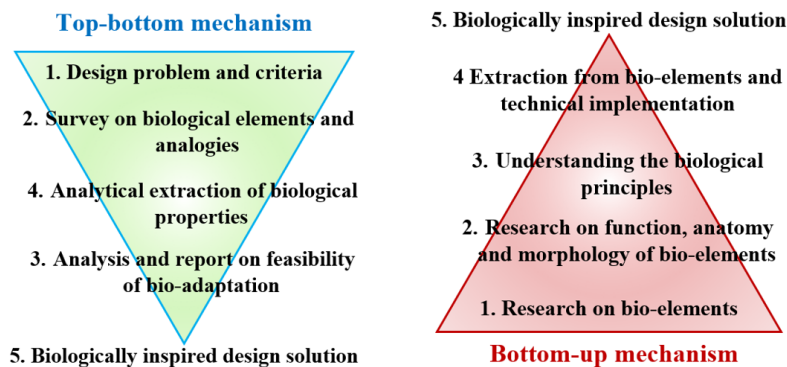


**Figure 1.** Top-bottom and Bottom-up principle to biomimicry.

Ideology and concept of biomimicry is being implemented in various fields of design such as architecture, textile industry, military technologies, biotechnology, aerodynamics-related technologies and many more [12], [13]. Many of human greatest inventions and innovations are a form of direct or indirect extrapolation and imitation from nature. For example Wright brothers was inspired by the idea of bird gliding mechanism, which uses air current for aerodynamic lift generation, which inspired the creation of the airplane [14]. Arguably aerodynamics-related technologies are regarded as the best-known example of biomimicry design adaptation. In transport aerodynamics, the mechanism and morphology of living organisms were adapted to increase the efficiency of the desired mechanism. For example, Shinkansen bullet train design was inspired by the beak of kingfisher [15]. Box fish inspired the creation of low drag bionic cars [16], [17]. In spite of the credibility and potential exhibited by biomimicry, the practice of implementing biomimicry remains limited among researchers [18].

### Biological Inspiration Implementation in Wind Turbines

Engineers are continuously analyzing and examining biological elements in attempt to achieve a favourable bio-adapted design in order improve the efficiency of WT. Seidel et al. [19] stated that VAWT holds several advantages over HAWT; however the major drawback is the efficiency. Hence, the authors adapted the biomimicry technique in attempt to improve the performance of WT. The authors examined the biological factor in terms of aerodynamic attributes of several bio-elements; namely maple seed, *Triplaris samara* seeds and whale tubercle. The finite element analysis (FEA) via ABAQUS carried out by the researchers shows that the bio-adapted WT blade could withstand wind speed up to 55 m/s. Lentink et al. [20] investigated the aerodynamic attributes of auto-rotating seeds and leading-edge vortices (LEV) mechanisms. The author observed that while descending, the seeds generate a stable LEV, consequently increases the lift force. The author also mentioned that LEV's high lift generating mechanism not only can be observed in auto-rotating plants but also in insects, bats and birds. However, there is a major drawback to LEV mechanism, which is the lift to drag ratio (LDR). Naturally auto-rotating seeds LEV mechanism maximized LDR, which consequently increased drag [21]. Hence, this reflects that direct implementation of the LEV mechanism onto WT will reduce the efficiency. Therefore, a secondary biological element is required in order to comprehend the issue or, in other words, bio-hybridization of two or more bio-elements. Fish et al. [22] stated that geometrical properties of humpback whale tubercle of has the ability to maximise lift and reduce drag.

### Computer Vision based Image Extraction Process

Recently, with the advancement of computational capabilities, computer vision (CV) has grown into a versatile analytical tool for the investigation of raw image data. There are several domains to CV, namely image processing, machine learning, Artificial intelligence (AI) and computer graphics. However, image processing is widely endorsed by

researchers for fundamental groundwork. Image processing technique utilizes the morphological structure or feature of an image in order to identify its characteristics [23]. Morphological filters is utilized to sharpen and enhance images [24]. Lately, pattern recognition and image processing has grown significantly popular method among researchers from various fields ranging from biomedical imaging, remote sensing, multimedia computing, image data communication and etc [25]. This methodology allows researchers to extract valuable and essential data from raw images. The complex computational task of image processing ranges involves image warping, extracting and analysis shape, masking, and image statistical calculation and so on. Meanwhile, pattern recognition is based on an algorithm utilized for the process, which often regarded as part AI [26], [27]. Conventionally, image processing and pattern recognition often work hand in hand to resolve complex image acquisition task [25]. In general principal, image processing is executed based on fundamental predefined steps, as shown in Figure 2.

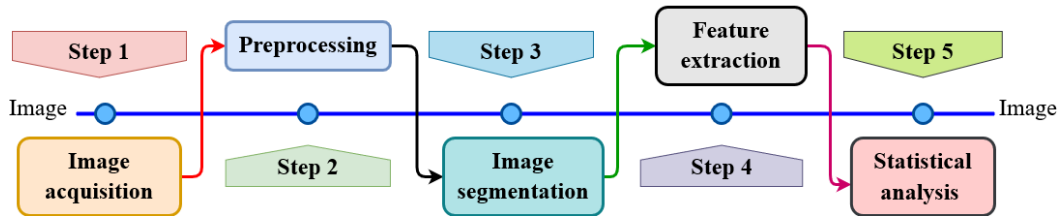


Figure 2. General methodology of image processing.

Although image processing is well verse and capable to operate in real-time [28], [29] and offline [30], however, there are factors such as noise [31], hardware processing capabilities [32], robustness of algorithm [33], and accuracy-precision [34]. Hence, in order to counter this issues, developers and researches adapt different technique namely filters, specialized algorithm. Case in point, convolution filter is utilized for images with low brightness and depixelated, where the original brightness of a pixel is replaced with the computed brightens value of eight neighboring pixels [35]. On the other hand, the edge detection algorithm is widely utilized technique for various applications in image processing relative to shape or morphological detection. Initially, the theory of edge detection based on zero-crossing of Laplacian of Gaussian of an image was introduced by Marr and Hildreth [36]. The working principle of edge detection algorithm is that the intensity value of the neighboring pixels is compared; therefore the changes in density are named as edge region [37]. Kulyukin and Blay [38] stated that the edge detection algorithm converts an image into bitmap in which the algorithm utilizes canny edge detector. Once the edge is detected, the image undergoes Hough transform (HT) process in order to detect lines. Hough introduced HT for the purpose of bubble tracks, however it indicate great potential as an image processing algorithm [39]. In regards to line detection the mathematical definition HT is similar to Radon transform. Meanwhile in terms of noisy pixel present in raw image can be resolved via various denoising algorithms. However, it is troublesome to utilize the appropriate algorithm for denoising of the image with Gaussian noise, impulse noise or even hybrid of them [31].

## GENERAL METHODOLOGY OF BIO HYBRIDIZATION PROCESS

The biomimicry technique is adapted for the modelling process of SWT blade morphology based on the developed bio-hybridization process assisted by PyCharm and OpenCV. The design objective is broken-down to aerodynamic dominance effect of the WT system namely drag. The bio-elements are chosen accordingly relative to their aerodynamic properties. The aerodynamic properties of the selected bio-elements are investigated at the rudimentary stage in order to acknowledge the feasibility of design synthetization. At this stage, the finalized bio-elements undergo contour-feature extraction using OpenCV via Pycharm IDE. The image processing algorithm library in OpenCV is utilized to extract the outline contour of the image. The high-resolution images are converted into a binary image or in other words, grayscale in order to reduce background noise that impacts the extraction process. Recommended threshold values are utilized to simplify the visual data for analysis, such as image segmentation and morphological transformation. Concurrently, the estimated 2D outline morphology of the bio-elements is mathematically analysed in order to extract and represent the morphology numerically. Figure 3 shows the methodological design process flow.

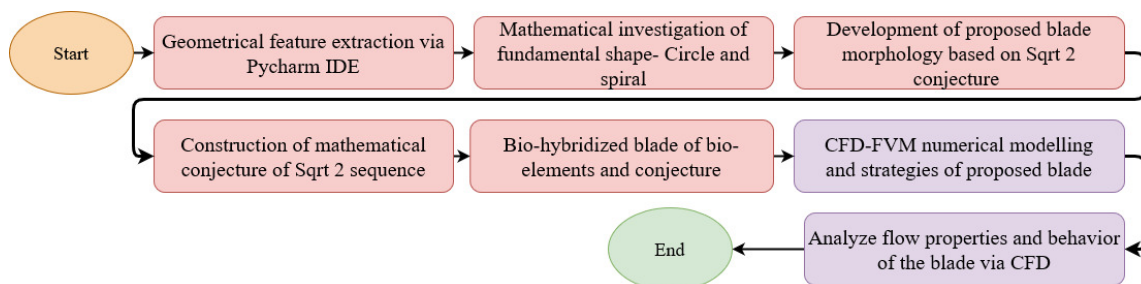


Figure 3. General design process flow.

The fundamental principle of bio-hybridization process is to improve the blade morphology and enhance the aerodynamic attributes (drag). Preliminary investigation of conventional straight blade semi-circular SWT [40] indicated that the height of blade semi-circular curvature impacted the performance of the turbine in terms of torque. Hence, the blade curvature reduction process is implemented. The proposed blade curvature with lower blade height is inspired by Nautilus shell and spiral configuration (Mathematical representation). Although the proposed design outperformed conventional SWT, the overall percentage of improvement in terms of moment coefficient ( $C_m$ ) is not significant. Therefore, in this study secondary stage of the bio-hybridization process is implemented to improve the drag attributes and flow characteristics. Moreover, the geometry of semi-circle and spiral configuration is analysed in order to obtain mathematical correlation and theories. The properties gathered of the mathematical analysis is utilized for the development of proposed conjecture. Right after the mathematical analysis, the morphology bio-elements are synthesized into the construction of VAWT blade. The behaviour of the bio-adapted blade morphology is investigated via rudimentary CFD analysis in order to formulate the aerodynamic behaviour [40].

### Bio-Elements Morphological Properties

Bio-elements are selected based on their aerodynamic attributes and geometrical feature. The design hybridization process is achieved by the combination of non-aerodynamic and aerodynamic bio-element. The non-aerodynamic bio-element is adapted for the blade morphing process where else the aerodynamic bio-element is utilized for the enhancement of aerodynamic factor with regards to type of WT. Table 1 shows the adapted bio-elements for this study. The extracted morphology of the bio-elements is numerically and computationally analysed. As reported in Table 1, the WT system is classified into two groups based on its aerodynamic dominance, namely drag and lift. The WT design process is carried out in two stages; the primary and secondary stage. The primary stage of the design process is the construction of the mainframe of the blade shape. The secondary is the construction and implementation of bio-elements for the enhancement of aerodynamic properties. The property and behaviour of the chosen bio-elements is based on the literature provided by researcher on their respective studies. The design hybridization is carried out based on top-bottom mechanism, where the bio-adaptation process is initiated by design problem and criteria.

The selected bio-elements are reconfigured and altered in order to fit the design problem and criteria of WT. Besides, three levels of biomimicry are utilized namely organism, behaviour and ecosystem of the selected bio-elements is utilized to approach the design problem. Moreover, the presented geometries are geometrically analysed in mathematical terms. The configuration of the adapted bio-system is analysed in terms of CFD and EFD to ensure the credibility of the proposed design. However, the presented design is scrutinized based on the result obtained via EFD and CFD for optimization.

**Table 1.** Chosen bio-elements for bio-hybridization process

WT blade system	Aerodynamic bio-elements	Non-aerodynamic bio-elements
Drag induced (DIWT)	Barnacle morphology and ecosystem behaviour.	Nautilus shell morphology and spiral configuration.

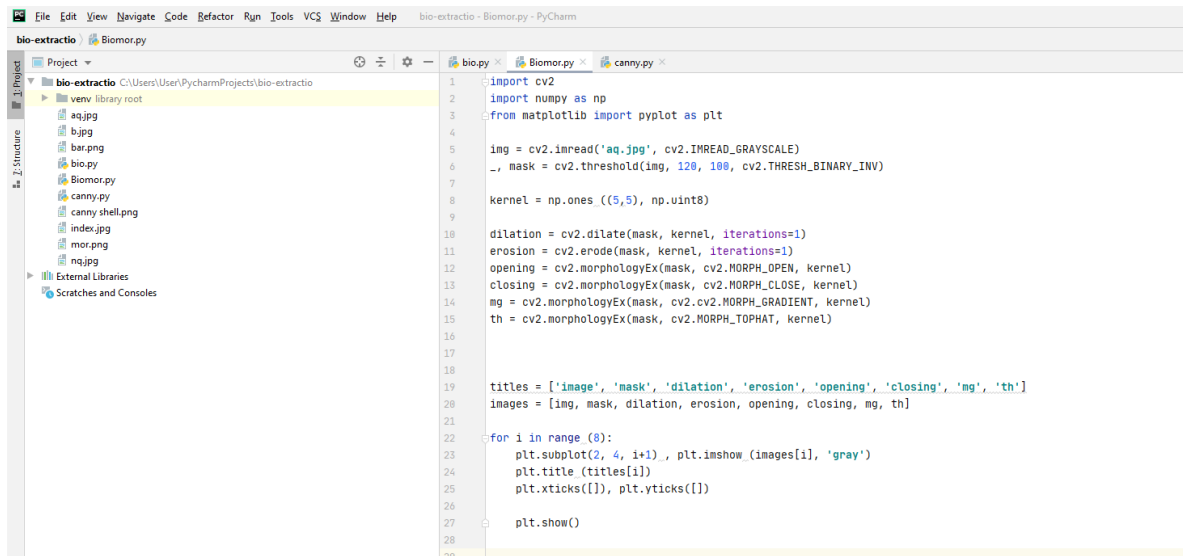
### Image Processing via OpenCV

Since the study involves analysing and recognizing complex morphologies of bio-elements, a computational-based framework is utilized for the geometry extraction process. The adapted computational framework is computer vision [41]; it is an interdisciplinary field of science, technology and engineering based on image processing technique [42] where a digital image and video are interpreted and analysed via executed programmed command. Computer vision based image processing technique can be executed in several platform namely Matlab (Matrix Laboratory) [43], [44], OpenCV (Open-source computer vision) [45], [46], CUDA [47], [48], TensorFlow [49], [50] and SimpleCV [51]. Despite the fact that there are several software for image processing applications, Matlab is widely recommended and prominent among researchers because of its stable, extensive and strong mathematical and numerical toolbox support for the execution of advanced and complex algorithms. However, Matlab is a high price commercially available software and consumes a large amount of computational power. Therefore, free of cost platform namely OpenCV-PyCharm is considered for this study. OpenCV is an open-source architecture based on C++ developed by Intel, under BSD (Berkeley software distribution) license. Moreover, endorse the fact that OpenCV is faster in processing and rendering selected complex algorithm in contrast to Matlab.

Elsayed and Yousef [52] carried out speed comparative investigation on Matlab and OpenCV based on machine learning algorithms. It is found that, OpenCV outperformed Matlab in terms of performance, where the speed ratio is more than 80 in some datasheet cases. Therefore, OpenCV software library is chosen to proceed with the execution of image processing procedure. OpenCV cross platform library requires an integrated development environment (IDE) platform in order to execute the image processing task. Therefore, open-source IDE and widely recommended platform is utilized; namely PyCharm. Python software is integrated with de facto standard package management system namely pip. Hence, pip manage and install additional packages installed via command. In this study the additional packages for image processing are OpenCV, Matplotlib and NumPy. Figure 4 shows the interface of PyCharm IDE. Prior to proceeding into geometrical contour detection, digital images as shown are surveyed and assessed in order to meet the requirement of high quality image.

Bernasconi [53] stated that the quality of the digital image dictates the reliability of the result produced by image processing. A high-quality picture means that the chosen images are in high resolution with minimal background noise in order for the algorithm to accurately extract the digital data. In addition to that, the OpenCV color conversion command

of the images is executed to ensure the packages is properly installed. Moving into the procedure, the original color image is converted into gray scale, this is due to the color noise presented by the colored image, as shown in Figure 5. Since the objective of the task is to detect edges and contour of the object in the image, it is difficult for the algorithm to detect in hue mode than in grayscale. Moreover, the computational resources will execute the process faster in gray scale mode than in color. The grayscale image is then converted into binary image in to remove to further remove the background noise. Moreover, in order to proceed into morphological transformation operations, the image is needed to be converted into binary image. Morphological transformation [54] is categorized into seven types namely dilation, morphological transformation, opening, erosion, closing, top hat and black hat. The quality of the operations is dependent on two input namely the original image and structuring element or kernel [54]. Kernel is a matrix form that dictates the nature of the operations; it is widely used for transformation techniques. The quality of the output image is securitized; it is found that morphology gradient operation produced a better result in contrast to the counterparts, as shown Figure 6.



```

1 import cv2
2 import numpy as np
3 from matplotlib import pyplot as plt
4
5 img = cv2.imread('aq.jpg', cv2.IMREAD_GRAYSCALE)
6 _, mask = cv2.threshold(img, 120, 100, cv2.THRESH_BINARY_INV)
7
8 kernel = np.ones((5,5), np.uint8)
9
10 dilation = cv2.dilate(mask, kernel, iterations=1)
11 erosion = cv2.erode(mask, kernel, iterations=1)
12 opening = cv2.morphologyEx(mask, cv2.MORPH_OPEN, kernel)
13 closing = cv2.morphologyEx(mask, cv2.MORPH_CLOSE, kernel)
14 mg = cv2.morphologyEx(mask, cv2.MORPH_GRADIENT, kernel)
15 th = cv2.morphologyEx(mask, cv2.MORPH_TOPHAT, kernel)
16
17
18
19 titles = ['image', 'mask', 'dilation', 'erosion', 'opening', 'closing', 'mg', 'th']
20 images = [img, mask, dilation, erosion, opening, closing, mg, th]
21
22 for i in range(8):
23     plt.subplot(2, 4, i+1), plt.imshow(images[i], 'gray')
24     plt.title(titles[i])
25     plt.xticks([], plt.yticks([]))
26
27 plt.show()
28
29

```

Figure 4. Interface of PyCharm IDE.

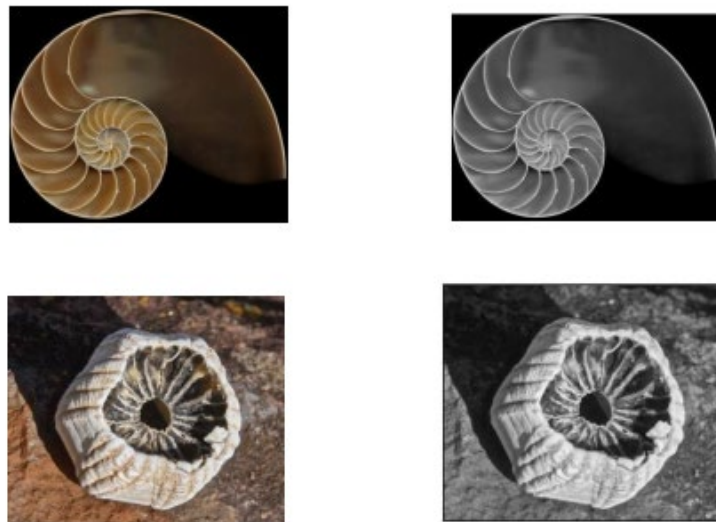
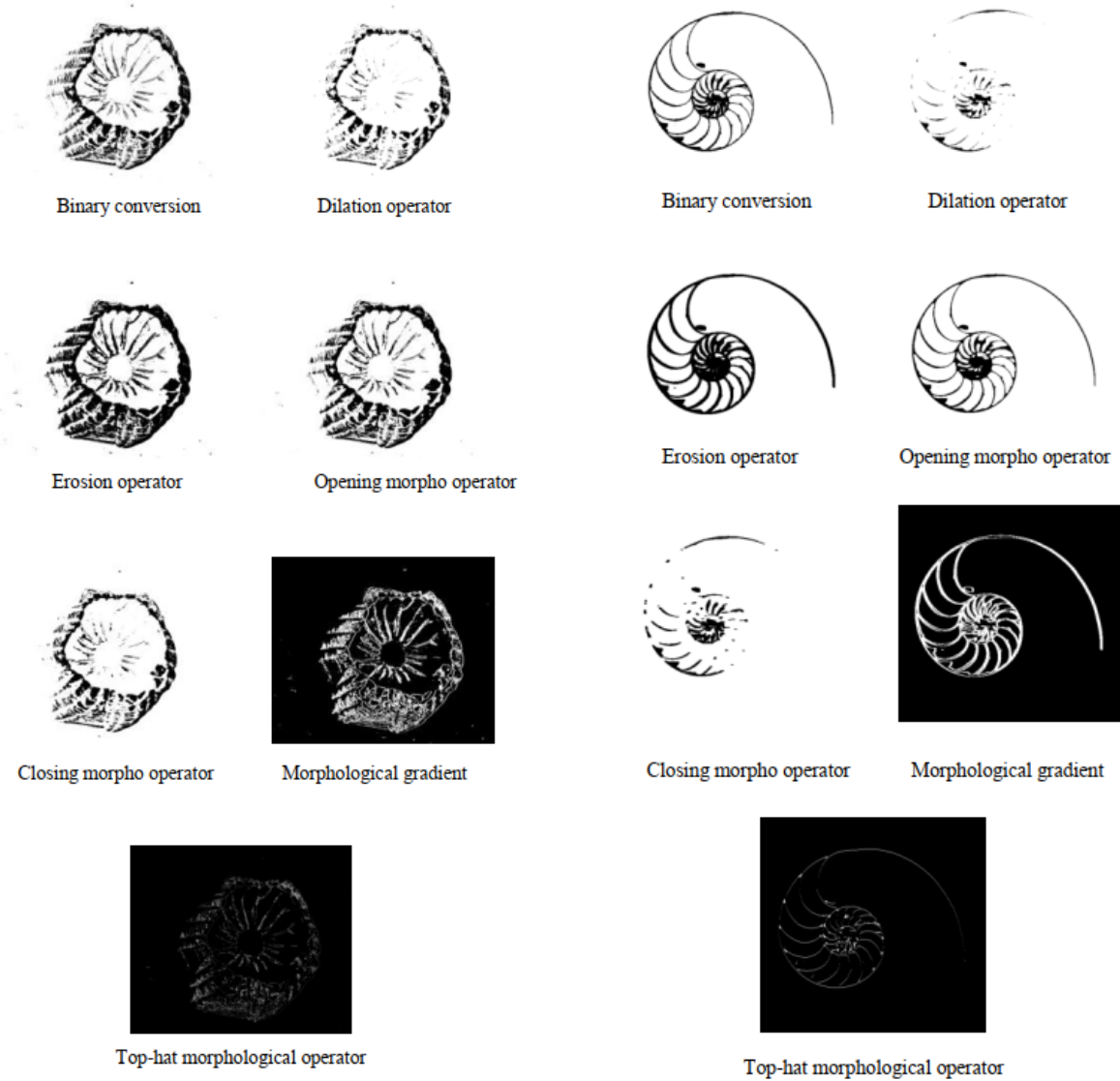
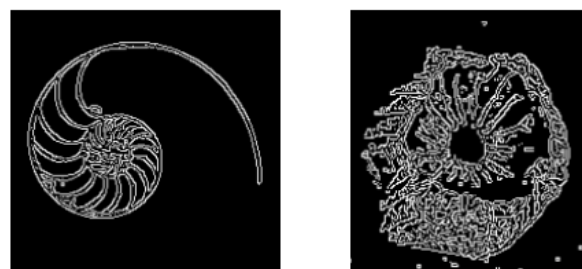


Figure 5. Conversion to grayscale via OpenCV-PyCharm.

A simple denoise algorithm is applied to the image in order to reduce the pixel noise presented in the image. In order to further suppress background noise, a smoothing or blurring technique via diverse linear filter is applied. The filters applied for the image are 2D-convolution, blur, and Gaussian blur. It is found that, qualitatively Gaussian blur suppressed more noises and much clearer in comparison to other filters. The quality of the image is further scrutinized to ensure minimal digital noise is present. It is necessary for the image to undergo multiple noise removal or denoising operation is because edge detection algorithm is susceptible to noise [54]. There are several methods in image processing for edge detection namely Laplacian, Sobel X & Y, Sobel combined and Canny edge detection. It is found that Canny edge detection is prominent and widely used. Hence, Canny edge detection algorithm is then utilized for edge detection operations. The threshold value is adjusted accordingly to satisfy the edge detected, the appropriate values are 100, 200 as shown in Figure 7.



**Figure 6.** Morphological transformation using OpenCV-PyCharm.



**Figure 7.** Canny edge detection via OpenCV-PyCharm.

### Outcome of Mathematical Analysis of Circle and Spiral

The aim of primary stage of the design process is to construct the mainframe of the WT blade shape, which is extracted from a non-aerodynamic element which is Nautilus shell. However, in order to meet the requirement of design criteria, the outline morphology of nautilus shell is mathematically and computationally investigated. The semi-circular geometry of conventional SWT is set as a reference in the design process of the proposed shape. Since the design criteria are to propose a blade morphology with enhanced aerodynamic performance in comparison to conventional SWT. Hence, the geometrical investigation is carried out in order to find the numerical factor that influences the building block of semi-circular shape. The geometrical investigation is carried out in terms of Euclidian geometry based on metallic ratios. The gather information from the geometrical investigation is utilized to develop a shape-driven conjecture in order to understand the governing factors of geometries. The extracted contour based on image processing is utilized for mathematical investigation of the geometry, namely spiral and circle [55]. Hence a mathematical conjecture is derived

based on the geometrical analysis as shown in Eq. (1). Previous preliminary 2D investigation of the blade constructed based on the conjecture has reduced the blade height which consequently improved the moment coefficient and rotational properties [40]. Moreover, based on the  $\sqrt{2}$  sequence it is found that the newly found conjecture is able to create multiple blade curvature.

$$\text{Proposed conjecture} = \sqrt{2}, \sqrt{2} + 1, \sqrt{2} + 2 \quad (1)$$

### Design Configuration and Attributes of DIWT

The proposed DIWT is a result of hybridization of two bio-elements namely nautilus spiral configured shell and barnacle marine organism. Meanwhile in order to enhance the drag attributes of the proposed SWT blade, drag-inducing element is implemented on the blade surface. The element is inspired by the geometry exhibited by the barnacle marine organism as shown in Figure 8(a). In a marine ecosystem perspective, barnacle is a parasitic organism that latches upon the host to structurally benefit itself and expand its ecosystem. This parasitic mechanism is called bio-fouling, where a surface is occupied and covered by micro and macro organism and their by-product [56], [57]. Bio-fouling is considered an undesirable occurrence which results in techno-economic issues on industrial equipment [58] and harms other marine life like whales [59] and turtles [60]. Accumulation of marine organisms on the surface of ships is said to increase skin friction resistance and fuel consumption [61]. However, the magnitude rise in drag attributes is dependent on the coverage of barnacle by fouling process on the respective surface. It would be redundant and impossible to emulate the natural coverage pattern of barnacle since the fouling is based on numerous environmental factors and variables. Hence, coverage of barnacle is reconfigured in order to adapt to WT blade surface and design criteria. As shown in Figure 8(b), the barnacle geometries are aligned on the blade surface in a linear pattern for the preliminary stage of CFD analysis. For simplicity, the parametric design attributes of the proposed design are similar to conventional SWT design in terms of overlap and aspect ratio. On the other hand, in terms of blade configuration, the proposed design is modelled as a single stage with two straight blades WT without the presence of endplates. Figure 9 shows the PLA based 3D printed proposed DIWT. The bio-adaptation is carried out in two stages, where the primary stage of the hybridization process is the blade curvature configuration as non-aerodynamic element which is inspired by Nautilus shell. Meanwhile, the second stage bio-adaptation is the aerodynamic attributes inspired by barnacle organism, where the geometrical feature is intended to be utilized to amplify drag.

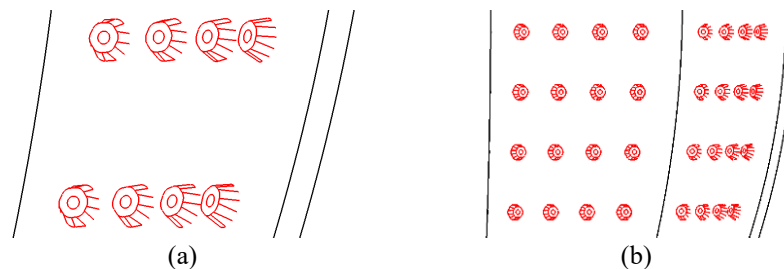


**Figure 8.** Second stage of design process: (a) barnacle inspired blade surface, (b) linear alignment of barnacle geometry on blade surface.

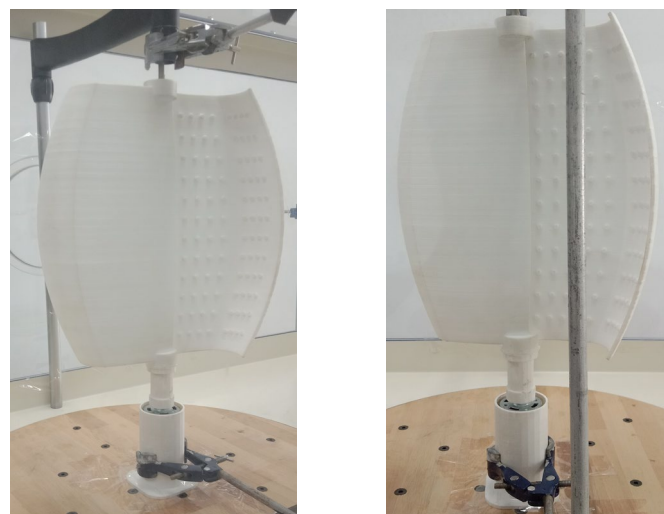


**Figure 9.** PLA 3D printed proposed DIWT.

### Parametric Attributes of DIWT

Moreover, the blade profile of DIWT is constructed, curving outwards in the parabolic configuration as opposed to straight SWT blade. Figure 10 shows the parabolic shape profile of the blade. The turbine is composed of two blades with

no endplates in SWT configuration. The labelled WT parametric attributes of the proposed rotor are shown in Figure 10. Meanwhile, the configuration of the barnacle-inspired microstructures is aligned in a non-linear configuration on the surface of the blade. Each blade is composed of 108 barnacle microstructures, as shown in Figure 10. The spacing between the barnacle microstructures is non-linear due to the blade curvature of tail and main curve. As reported in Table 2, the parametric attributes of the proposed design are labelled into 6, namely blade profile height ( $H$ ) with 0.28 m, rotor diameter ( $D_r$ ) at 0.26 m, blade diameter ( $d$ ) at 0.142, shape diameter ( $b$ ) is 0.0062 m, and overlap region ( $O$ ) is at 0.028 m. Based on the constructed parametric attributes, other WT properties like aspect ratio ( $A.R$ ), swept area ( $S_A$ ) and overlap ratio ( $OR$ ) are numerated using Eq. (2) to (4). Where the  $A.R = 1.08$ ,  $S_A = 0.067$  and  $OR = 0.153$ . Table 3 reports the configuration attributes of the proposed DIWT. The blade shape mainframe which is utilized to construct the blade profile, consists of two segments of non-uniform geometry namely main curve and tail curve, as illustrated in Figure 11. As for the morphology of the proposed design, the top-bottom bio-adaptation technique is implemented for the construction of the blade as shown in Figure 11. Moreover, the governing numerical factor namely the proposed conjecture, is utilized as the primary tool for the construction of the curvature of the blade. Thus, indicating that the proposed design is at the preliminary stage of parametric modelling.

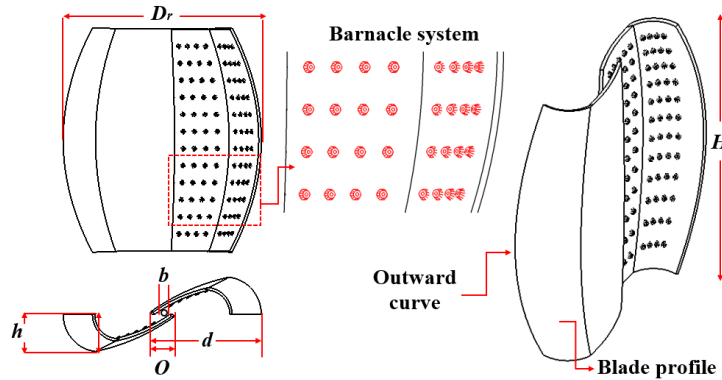


Figure 10. Schematic on proposed design configuration.

Table 2. Parametric attributes of proposed DIWT.

Turbine	$H$ (m)	$D_r$ (m)	$d$ (m)	$O$ (m)	$h$ (m)	$b$ (m)
Proposed turbine	0.28	0.26	0.142	0.028	0.044	0.0062

$$A.R = \frac{H}{D_r} \tag{2}$$

$$S_A = D_r \times H \tag{3}$$

$$O.R = \frac{O - b}{d} \tag{4}$$

Table 3. Configuration attributes of DIWT.

Turbine	$A.R$	$S_A$ (m)	$OR$
Proposed turbine	1.08	0.067	0.153

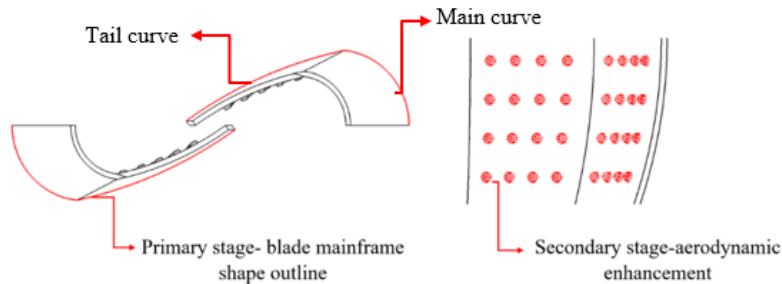


Figure 11. Primary and secondary stage of adaptation in design configuration.

## BRIEF DESCRIPTION OF NUMERICAL MODEL FRAMEWORK

The grid topology is discretized using the sliding mesh method (SSM) via non-conformal mesh configuration. The defined grid topology consists of highly unstructured mesh. Grid sensitivity study is conducted in order to obtain the

appropriate mesh resolution and configuration for minimal computational cost for numerical investigation without jeopardising the reliability of the result. The mesh mode utilized to analyse the proposed WT is a sliding grid between interfaces. The computational model is investigated at fine and medium mesh resolution in terms of  $C_m$ . The resulted  $C_m$  at different grid resolution is observed the discrepancy between fine and medium mesh densities. As shown in Table 4, under similar numerical solver parameter the WT is simulated at 6 m/s for 5 periods. Both mesh densities indicate good agreement with trivial dissimilarities under different number of elements, the number of elements for medium and fine mesh is 2031188 elements and 3458711 elements respectively. At medium-mesh resolution the output moment coefficient is  $C_m = 0.2272$ , while fine mesh resolution resulted in output of  $C_m = 0.2295$ . Due to the complexity presented by the geometry of the proposed WT, a denser mesh is noticeable along with the barnacle system on the blade surface. Hence, this design configuration inevitably consumes large computational cost in both mesh topology construction and simulation time regardless in medium or fine resolution. Therefore, body sizing at 0.001 m is utilized at different relevance centre value to generate fine and medium mesh topology. Grid convergence test is conducted using  $C_m$  as the variable to analyse the influence of number of elements on the sensitivity of the computed variable, as shown in Figure 12. The simulation time for medium and fine resolution is 3 days 5 hrs and 4 days 27 min, respectively. Hence, medium mesh resolution is chosen for the rest of the simulation.

In a nutshell, the numerical model is executed based on unsteady Reynolds averaged Navier-Stokes equation (URANS) as shown in Eq. (5) The 3D simulation is conducted in transient state. Similar solver configuration and CFX expression language (CEL) is utilized to express the relevant equations. The simulations are conducted in high-order scheme based on two-equation turbulent transport model (SST  $k-\omega$ ) as shown in Eq. (6). Table 5 reports the boundary condition and solver configuration for simulation conducted in Ansys CFX 15. In order to minimize computational cost for preliminary investigation, the number of time step is reduced to 50.

**Table 4.** Grid independence test between fine and medium mesh density.

$U_\infty$ (m/s)	Mesh type	Number of nodes	Number of elements	$C_m$
6.0	Medium	847038	2031188	0.2272
6.0	Fine	1117646	3458711	0.2295

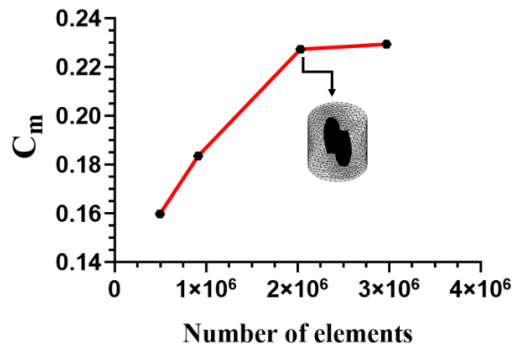


**Figure 12.** Grid convergence test.

**Table 5.** Boundary condition parameters.

Boundary condition	Parameter	Value
Boundary condition type	Neumann condition	-
Cell zone condition	Air @ 25 ° C	$\rho = 1.1871 \text{ kg / m}^3$
Blade wall type	No slip condition	-
Outlet	Pressure outlet	0-Pascal
Hydraulic diameter, $D_h$	Rectangular geometry (Test section)	0.6 m
Tube wall condition	No-slip condition-stationary wall	-

Reynolds decomposition,

$$u(x, y, t) = \bar{u}(x, y) + u'(x, y, t) \tag{5}$$

SST  $k-\omega$ ,

$$\frac{\partial}{\partial t}(\rho\omega) + \frac{\partial}{\partial x_i}(\rho\omega u_i) = \frac{\partial}{\partial x_j} \left( \Gamma_\omega \frac{\partial \omega}{\partial x_j} \right) + G_k - Y_\omega + D_\omega + S_\omega \tag{6}$$

## RESULTS AND DISCUSSION ON PROPOSED DESIGN PERFORMANCE

The preliminary configuration of the proposed design is investigated in terms of CFD in relation to experimental measurement and design feature. A similar discretised mesh topology which is verified via grid sensitivity study, is utilized to analyse the WT at wider  $\lambda$  ranging from  $\lambda = 0.5 - 0.7$  at 7 m/s in terms of  $C_m$ . The aim of this preliminary numerical investigation is to study the behaviour of the WT in response to the design configuration and flow condition. As shown in Figure 13, the numerical oscillation of  $C_m @ \lambda = 0.2$  indicated quasi-steady convergence by time. Hence this indicates that the utilized numerical method did not exhibit or amplify noises at the defined conditions. However, sharp edges at the crest and trough of the waveform cycle can be observed, this is due to the time-step size.

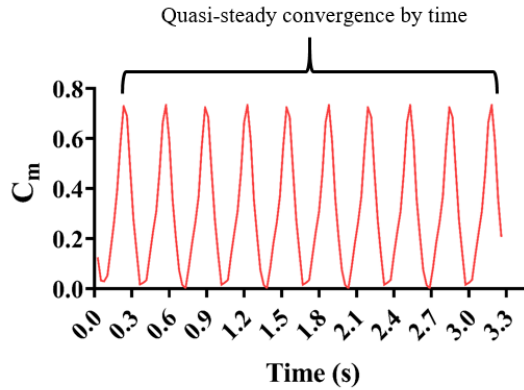


**Figure 13.** Quasi-steady convergence of CFD numerical model.

As can be observed in Figure 14, the  $C_m$  of the proposed design decreases relative to the increase of  $\lambda$  at 7 m/s. It is observed that there are several motivating factors that affected the performance of the WT. The motivating factors are analysed in terms of design configuration and dynamic flow factors. In order to obtain the variation in RPM and  $\lambda$  at 7 m/s for executing the numerical investigation, load variation technique is applied. However, due to the unavailability of load adjusting mechanism namely load-spring balance system, the load on the WT is manual adjusted. Since the sole purpose in this section is to investigate the behaviour of the WT configuration in response to the upwind, methods on experimental uncertainty are calculated nor applied. Based on the result shown in Figure 14, the peak  $C_m$  is at  $\lambda = 0.55$  for experimental and CFD is  $C_m = 0.238$  and  $C_m = 0.253$  respectively. The result is then compared with conventional SWT. However, research data on SWT configuration with similar dimensions and experimental parameter to the proposed design is unavailable. Therefore, experimental research conducted by Jeon et al. [62] and Mahmoud et al. [63] utilized as a reference to evaluate the performance of the proposed design. However, the SWT configuration presented by the authors is in different dimension [63], helical or twisted blade [62] and experimental wind conditions. Regardless the configuration and dimension, the data on SWT can be utilized for evaluation of the performance of drag-driven WT in general terms. Since Mahmoud et al. [63] presented data on the performance of the rotor power ( $P_r$ ), Equation 7 is utilized to convert into  $C_p$ . Moreover, get data graph digitizer is utilized to extract data from the presented result by the authors. The presented SWT configuration by Jeon et al. [62] resulted in  $C_p = 0.141$  which is  $D_r = 250$  mm, where else the proposed design resulted in experimental and numerical  $C_p = 0.113$  and  $C_p = 0.127$  respectively at 7 m/s and  $\lambda = 0.7$  as shown in Figure 15. Meanwhile, Mahmoud et al. [63] mention that for straight blade SWT at 6 m/s the  $C_p = 0.011$ . Since the mainframe of the paper is to propose a geometrical technique for the construction drag driven wind turbine blade, the difference between CFD and experimental result and trend behavior is not presented in this paper.

$$C_p = \frac{M\omega}{\frac{1}{2}\rho Av^3} \tag{7}$$

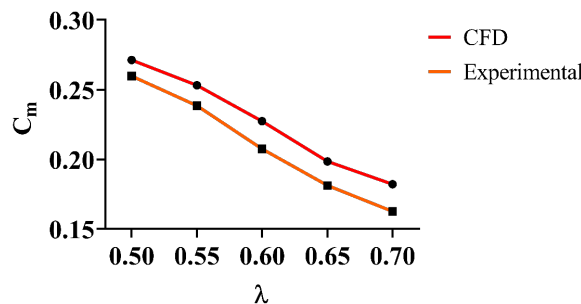


**Figure 14.** Moment coefficient vs tip speed ratio at 7 m/s.

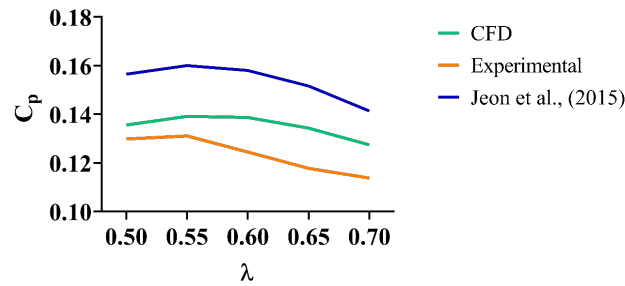


**Figure 15.** Power extraction coefficient vs  $\lambda$  at 7 m/s.

Moreover, based on the proposed DOA, it is found that the implementation of barnacle-inspired geometry on the surface on the rotor reduces the magnitude of pressure distribution. The reduction of pressure distribution on advancing blade in contrast to returning blade effects the aerodynamic torque of the rotor. Due to the implementation of the barnacle geometry, this resulted the blade to experience early flow separation. Consequently, it induced an intense, unstable wake region compared to rotor without barnacle as shown in Figure 16(a) and 16(b). It is evident that the instability exhibited by the flow response with intense vortex shedding has disrupted the flow effects for an effective torque distribution. Moreover, it is noticeable high-velocity flow region at the tip of the advancing blade of the proposed design with barnacle contributed for the poor pressure distribution compared to design without barnacle, as shown in Figure 16(a) and 16(b). Since the wake region passively dictates the flow properties of the returning blade [64]. Conventionally, the dynamic effects of the traditional SWT rotor governs the pressures distribution of the returning blade, which causes flow separation to occur drastically that eventually reduces the drag force of the returning blade [65]. Moreover, the traditional rotor experiences a rise in pressure behind the returning blade in contrast to the front side. Comparatively, the intensity of the pressure distribution of the advancing blade must be greater than the returning blade into initiate a stable angular rotation relative to the upwind. This is due to the decrease in drag force of the returning blade which provides a significant pressure drag difference between the blades. Ultimately, this occurrence provides positive torque distribution for SWT rotor.

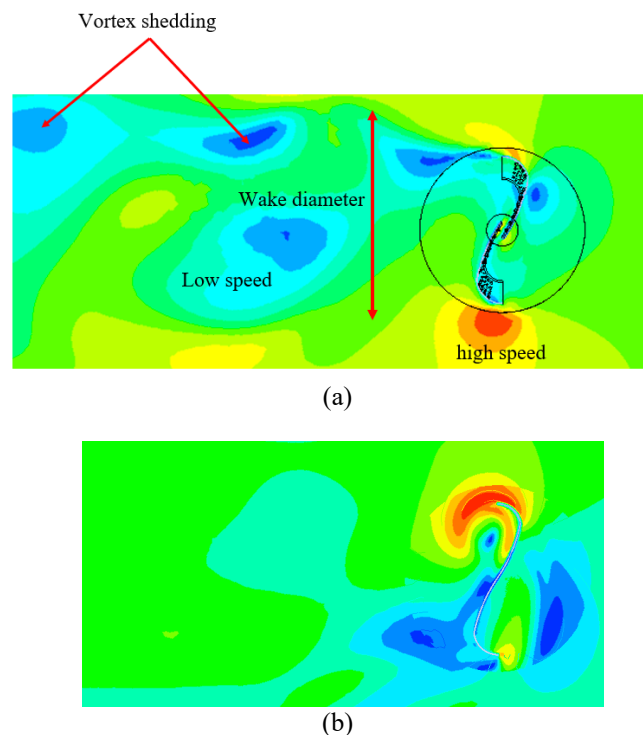


**Figure 16.** Flow properties of proposed design at 6 m/s. (a) Velocity magnitude of proposed design with barnacle, (b) Velocity magnitude of proposed design (no barnacle)

However relative to the proposed design, the pressure distribution behind returning blade located at the curvature is higher than the advancing blade as shown in Figure 17(a) and 17(b). The barnacle geometry and its configuration introduces early turbulence and consequently reduces the pressure drag. Moreover, the barnacle configuration increases viscous drag emulating vortex generators mechanism. Since the body is in rotating motion the generated turbulent regime effected the subsequent blade. It is observed during experimental procedure the proposed configuration led to flow instability and vibration even at low speed. Moreover, it is noticeable in Figure 16(a) the reduced in velocity behind the returning blade contributes to the rise in pressure. The close arrangement of the barnacle system converges the separated flow whereby amplifying the kinetic energy of the fluid which can be observed in flow attachment as shown in Figure

16(a). Therefore, reduction in pressure in front and back of the advancing blade in return reduces the pressure drag, hence reduces the effectiveness in torque distribution. Since there is no significant difference in terms of pressure drag of the returning and advancing blade, which consequently impacted the performance in terms of  $C_p$  and  $C_m$  of the proposed design.

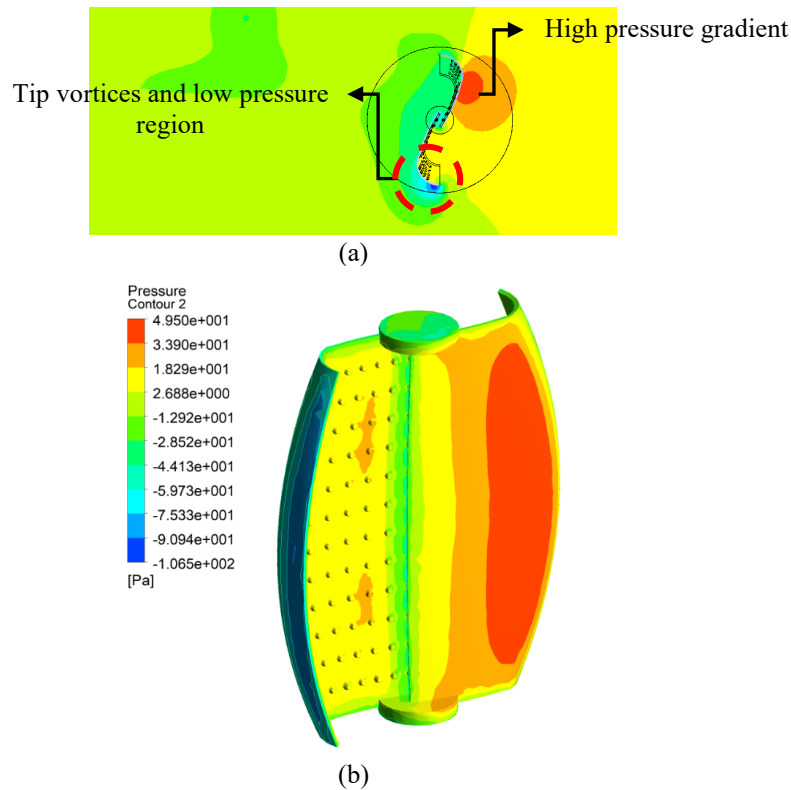


**Figure 17.** Proposed design with barnacle. (a) Pressure distribution contour, (b) 3D rotor pressure distribution

## CONCLUSION

This manuscript presents a novel geometrical design strategy for drag driven WT based on mathematical conjecture, image processing through OpenCV and bio-hybridization. The validity of the approach is mainly investigated via CFD numerical model. Result shows that the selected bio-element namely barnacle is not appropriate for integration of drag driven WT design. This is due to the barnacle geometry and its configuration which introduces early turbulence and consequently reduces the pressure drag. Moreover, the barnacle configuration increases viscous drag emulating vortex generators mechanism. Since the body is in rotating motion the generated turbulent regime effected the subsequent blade. The peak  $C_m$  is at  $\lambda = 0.55$  for experimental and CFD is  $C_m = 0.238$  and  $C_m = 0.253$  respectively. The literature based SWT configuration resulted in  $C_p = 0.141$  which is  $D_r = 250$  mm, where else the proposed design resulted in experimental and numerical  $C_p = 0.113$  and  $C_p = 0.127$  respectively at  $7$  m/s and  $\lambda = 0.7$ . It is concluded that integration of barnacle on the blade surface is not suitable for drag driven wind turbine. However, previous investigation the blade curvature (without barnacle) derived from the mathematical conjecture improves the rotational properties of the rotor compared to conventional SWT. This is evident that the outcome of the mathematical analysis provides an alternative approach in blade mainframe reconfiguration. The outcome of this preliminary investigation is adapted for future design reconfiguration and optimization. The conjecture and geometrical design strategy will be tested in the construction of hydrokinetic or other turbomachinery in order to observe the behavior of the blade. Moreover appropriate optimization strategy need to be utilized to investigate the proposed design strategy in order to obtain constructive results. The proposed design approach provides an intuitive, systematic and structured technique for WT blade modelling. The presented technique with appropriate design bio-element couple with mathematical investigation of benchmarked morphology and image processing via OpenCV provides a reliable platform for engineers to model a practical WT blade morphology.

## ACKNOWLEDGEMENT

This research work was conducted under Fundamental Research Grant Scheme FRGS/1/2019/TK10/UMP/02/4 (UMP ref. RDU1901131). We would like to thank Ministry of Higher Education, Malaysia for making this research possible.

## REFERENCES

- [1] M. Gejdoš, Z. Tončíková, M. Němec, M. Chovan, and T. Gergel, "Balcony cultivator: New biomimicry design approach in the sustainable device," *Futures*, vol. 98, no. February 2017, pp. 32–40, 2018, doi: 10.1016/j.futures.2017.12.008.

- [2] M. S. Aziz and A. Y. El Sherif, "Biomimicry as an approach for bio-inspired structure with the aid of computation," *Alexandria Eng. J.*, vol. 55, no. 1, pp. 707–714, 2016, doi: 10.1016/j.aej.2015.10.015.
- [3] J. M. Benyus, *Biomimicry: Innovation Inspired By Nature*. New York: Morrow: HarperCollins, 1997.
- [4] N. Taylor Buck, "The art of imitating life: The potential contribution of biomimicry in shaping the future of our cities," *Environ. Plan. B Urban Anal. City Sci.*, vol. 44, no. 1, pp. 120–140, Oct. 2015, doi: 10.1177/0265813515611417.
- [5] H. Gitano-Briggs, "Low Speed Wind Turbine Design," in *Advances in Wind Power*, Rijeka: InTech, 2012.
- [6] P. J. Schubel and R. J. Crossley, "Wind Turbine Blade Design," *Energies*, vol. 5, no. 9, pp. 3425–3449, Sep. 2012, doi: 10.3390/en5093425.
- [7] W. Tong, *Wind Power Generation and Wind Turbine Design*. Kollmorgen Corporation, USA: WIT Transactions on State-of-the-art in Science and Engineering, 2010.
- [8] W. Zhang, C. D. Markfort, and F. Porté-Agel, "Near-wake flow structure downwind of a wind turbine in a turbulent boundary layer," *Exp. Fluids*, vol. 52, no. 5, pp. 1219–1235, May 2012, doi: 10.1007/s00348-011-1250-8.
- [9] P. J. Schubel and R. J. Crossley, "Wind turbine blade design," *Wind Turbine Technol. Princ. Des.*, pp. 1–34, 2014, doi: 10.1201/b16587.
- [10] J. N. Leonard, B. R. Fritz, L. E. Timmerman, N. M. Daringer, and M. C. Jewett, "Biology by design: From top to bottom and back," *J. Biomed. Biotechnol.*, vol. 2010, 2010, doi: 10.1155/2010/232016.
- [11] S. Pathak, "Biomimicry: (Innovation Inspired by Nature)," *Int. J. New Technol. Res.*, vol. 5, no. 6, pp. 34–38, 2019, doi: 10.31871/ijntr.5.6.17.
- [12] K. Hargroves and M. Smith, "Innovation inspired by nature: Biomimicry," *Ecos Sci. Sustain.*, no. 129, pp. 27–29, 2006, doi: 10.1071/EC129p27.
- [13] L. Eadie and T. K. Ghosh, "Biomimicry in textiles: Past, present and potential. An overview," *J. R. Soc. Interface*, vol. 8, no. 59, pp. 761–775, 2011, doi: 10.1098/rsif.2010.0487.
- [14] M. J. Eggermont, "Biomimetics as problem-solving, creativity and innovation tool in a first year engineering design and communication course," in *Design and Nature IV*, Jun. 2008, vol. I, pp. 59–67, doi: 10.2495/DN080071.
- [15] E. B. Kennedy and T. A. Marting, "Biomimicry: Streamlining the front end of innovation for environmentally sustainable products," *Res. Technol. Manag.*, vol. 59, no. 4, pp. 40–48, 2016, doi: 10.1080/08956308.2016.1185342.
- [16] H. Chowdhury, R. Islam, M. Hussein, M. Zaid, B. Loganathan, and F. Alam, "Design of an energy efficient car by biomimicry of a boxfish," *Energy Procedia*, vol. 160, no. 2018, pp. 40–44, 2019, doi: 10.1016/j.egypro.2019.02.116.
- [17] A. Kozlov, H. Chowdhury, I. Mustary, B. Loganathan, and F. Alam, "Bio-inspired design: Aerodynamics of boxfish," *Procedia Eng.*, vol. 105, no. 1, pp. 323–328, 2015, doi: 10.1016/j.proeng.2015.05.007.
- [18] J. F. V. Vincent, O. A. Bogatyreva, N. R. Bogatyrev, A. Bowyer, and A. K. Pahl, "Biomimetics: Its practice and theory," *J. R. Soc. Interface*, vol. 3, no. 9, pp. 471–482, 2006, doi: 10.1098/rsif.2006.0127.
- [19] C. Seidel, S. Jayaram, L. Kunkel, and A. Mackowski, "Structural Analysis of Biologically Inspired Small Wind Turbine Blades," *Int. J. Mech. Mater. Eng.*, vol. 12, no. 1, p. 19, Dec. 2017, doi: 10.1186/s40712-017-0085-3.
- [20] D. Lentink, W. B. Dickson, J. L. Van Leeuwen, and M. H. Dickinson, "Leading-edge vortices elevate lift of autorotating plant seeds," *Science (80-. )*, vol. 324, no. 5933, pp. 1438–1440, Jun. 2009, doi: 10.1126/science.1174196.
- [21] C. Pandolfi and D. Izzo, "Biomimetics on seed dispersal: survey and insights for space exploration," *Bioinspir. Biomim.*, vol. 8, no. 2, p. 025003, May 2013, doi: 10.1088/1748-3182/8/2/025003.
- [22] F. E. Fish, P. W. Weber, M. M. Murray, and L. E. Howle, "The tubercles on humpback whales' flippers: Application of bio-inspired technology," in *Integrative and Comparative Biology*, Jul. 2011, vol. 51, no. 1, pp. 203–213, doi: 10.1093/icb/icr016.
- [23] U. Rajashekar, A. C. Bovik, D. Sage, M. Unser, L. J. Karam, and R. L. Lagendijk, "Image Processing Education," in *Handbook of Image and Video Processing*, A. C. Bovik, Ed. Burlington: Elsevier, 2005, pp. 73–95.
- [24] H. Kaur, J. Virmani, Kriti, and S. Thakur, "A genetic algorithm-based metaheuristic approach to customize a computer-aided classification system for enhanced screen film mammograms," in *U-Healthcare Monitoring Systems*, N. Dey, A. S. Ashour, S. J. Fong, and S. B. T.-U.-H. M. S. Borra, Eds. Elsevier, 2019, pp. 217–259.
- [25] Z. Du, "Image processing and pattern recognition in industrial engineering," *Sens. Rev.*, vol. 31, no. 2, Mar. 2011, doi: 10.1108/sr.2011.08731baa.002.
- [26] F. Fontanella, F. Colace, M. Molinaro, A. Scotto Di Freca, and F. Stanco, "Pattern recognition and artificial intelligence techniques for cultural heritage," *Pattern Recognit. Lett.*, vol. 138, pp. 23–29, Oct. 2020, doi: 10.1016/j.patrec.2020.06.018.
- [27] R. M. Golden, "Statistical Pattern Recognition," in *International Encyclopedia of the Social & Behavioral Sciences*, N. Smelser and P. Baltes, Eds. Oxford: Elsevier, 2001, pp. 15040–15044.
- [28] T. Seybold, B. Klässner, and W. Stechele, "Denoising camera data," in *Emerging Trends in Image Processing, Computer Vision and Pattern Recognition*, L. Deligiannidis and H. R. B. T.-E. T. in I. P. Arabnia Computer Vision and Pattern Recognition, Eds. Boston: Elsevier, 2015, pp. 3–17.
- [29] M. Meribout, M. Nakanishi, and T. Ogura, "Accurate and Real-time Image Processing on a New PC-compatible Board," *Real-Time Imaging*, vol. 8, no. 1, pp. 35–51, Feb. 2002, doi: 10.1006/rtim.2001.0269.
- [30] S. Sihmar and P. Sharma, "Image processing techniques for offline handwritten recognition," in *2016 3rd International Conference on Computing for Sustainable Global Development (INDIACom)*, 2016, pp. 4014–4018.
- [31] A. Awad, "Denoising images corrupted with impulse, Gaussian, or a mixture of impulse and Gaussian noise," *Eng. Sci. Technol. an Int. J.*, vol. 22, no. 3, pp. 746–753, Jun. 2019, doi: 10.1016/j.jestch.2019.01.012.
- [32] X. Feng, Y. Jiang, X. Yang, M. Du, and X. Li, "Computer vision algorithms and hardware implementations: A survey," *Integration*, vol. 69, pp. 309–320, Nov. 2019, doi: 10.1016/j.vlsi.2019.07.005.
- [33] G. Shi, R. Ranjan, and L. R. Khot, "Robust image processing algorithm for computational resource limited smart apple sunburn sensing system," *Inf. Process. Agric.*, vol. 7, no. 2, pp. 212–222, Jun. 2020, doi: 10.1016/j.inpa.2019.09.007.
- [34] M. Bould, S. Barnard, I. D. Learmonth, J. L. Cunningham, and J. R. Hardy, "Digital image analysis: improving accuracy and reproducibility of radiographic measurement," *Clin. Biomech.*, vol. 14, no. 6, pp. 434–437, Jul. 1999, doi: 10.1016/S0268-0033(98)00113-2.
- [35] M. Gilg, "Representation of Networks of Wireless Sensors with a Grayscale Image: Application to Routing," in *Building Wireless Sensor Networks*, S. B. T.-B. W. S. N. Femmam, Ed. Elsevier, 2017, pp. 31–66.

- [36] L. Ding and A. Goshtasby, "Computer Science and Engineering Department Wright State University," *Pattern Recognit.*, vol. 34, no. 34, pp. 721–725, 2000.
- [37] Ş. Öztürk and B. Akdemir, "Comparison of Edge Detection Algorithms for Texture Analysis on Glass Production," *Procedia - Soc. Behav. Sci.*, vol. 195, pp. 2675–2682, 2015, doi: 10.1016/j.sbspro.2015.06.477.
- [38] V. Kulyukin and C. Blay, "An algorithm for mobile vision-based localization of skewed nutrition labels that maximizes specificity," in *Emerging Trends in Image Processing, Computer Vision and Pattern Recognition*, L. Deligiannidis and H. R. B. T.-E. T. in I. P. Arabnia Computer Vision and Pattern Recognition, Eds. Boston: Elsevier, 2015, pp. 277–293.
- [39] M. S. Nixon and A. S. Aguado, "High-level feature extraction: fixed shape matching," in *Feature Extraction and Image Processing for Computer Vision*, M. S. Nixon and A. S. Aguado, Eds. Elsevier, 2020, pp. 223–290.
- [40] S. N. Ashwindran, A. A. Azizuddin, and A. N. Oumer, "A moment coefficient computational study of parametric drag-driven wind turbine at moderate tip speed ratios," *Aust. J. Mech. Eng.*, pp. 1–15, Jan. 2020, doi: 10.1080/14484846.2020.1714364.
- [41] H. Liu, "Introduction to Computer Vision on Mobile Devices," in *Facial Detection and Recognition on Mobile Devices*, Edinburgh: Elsevier, 2015, pp. 1–9.
- [42] E. A. B. da Silva and G. V. Mendonça, "Digital Image Processing," in *The Electrical Engineering Handbook*, W. Chen Ken, Ed. Burlington: Elsevier, 2005, pp. 891–910.
- [43] M. F. Bulbul, F. Badsha, and R. Islam, "Object Detection by Point Feature Matching using Matlab," *Adv. Image Video Process.*, vol. 5, no. 6, Dec. 2018, doi: 10.14738/aivp.66.5619.
- [44] P. I. Corke, "The machine vision toolbox - A MATLAB toolbox for vision and vision-based control," *IEEE Robot. Autom. Mag.*, vol. 12, no. 4, pp. 16–25, Dec. 2005, doi: 10.1109/MRA.2005.1577021.
- [45] I. Culjak, D. Abram, T. Pribanic, H. Dzapov, and M. Cifrek, "A brief introduction to OpenCV," in *2012 Proceedings of the 35th International Convention MIPRO*, 2012, pp. 1725–1730.
- [46] L. Triyono, E. H. Pratisto, S. A. T. Bawono, F. A. Purnomo, Y. Yudhanto, and B. Raharjo, "Sign Language Translator Application Using OpenCV," *IOP Conf. Ser. Mater. Sci. Eng.*, vol. 333, p. 012109, Mar. 2018, doi: 10.1088/1757-899X/333/1/012109.
- [47] C. Tsotskas, T. Kipouros, and A. M. Savill, "The Design and Implementation of a GPU-enabled Multi-objective Tabu-search Intended for Real World and High-dimensional Applications," *Procedia Comput. Sci.*, vol. 29, pp. 2152–2161, 2014, doi: 10.1016/j.procs.2014.05.200.
- [48] V. Jain and D. Patel, "A GPU Based Implementation of Robust Face Detection System," *Procedia Comput. Sci.*, vol. 87, pp. 156–163, 2016, doi: 10.1016/j.procs.2016.05.142.
- [49] L. Yuan, Z. Qu, Y. Zhao, H. Zhang, and Q. Nian, "A convolutional neural network based on TensorFlow for face recognition," in *2017 IEEE 2nd Advanced Information Technology, Electronic and Automation Control Conference (IAEAC)*, Mar. 2017, pp. 525–529, doi: 10.1109/IAEAC.2017.8054070.
- [50] A. Voulodimos, N. Doulamis, A. Doulamis, and E. Protopapadakis, "Deep Learning for Computer Vision: A Brief Review," *Comput. Intell. Neurosci.*, vol. 2018, pp. 1–13, 2018, doi: 10.1155/2018/7068349.
- [51] V. Menezes, V. Patchava, and M. S. D. Gupta, "Surveillance and monitoring system using Raspberry Pi and SimpleCV," in *2015 International Conference on Green Computing and Internet of Things (ICGCIoT)*, Oct. 2015, pp. 1276–1278, doi: 10.1109/ICGCIoT.2015.7380661.
- [52] A. A. Elsayed and W. A. Yousef, "Matlab vs. OpenCV: A Comparative Study of Different Machine Learning Algorithms," *arXiv Prepr. arXiv1905.01213*, pp. 1–6, May 2019, [Online]. Available: <http://arxiv.org/abs/1905.01213>.
- [53] A. Bernasconi, "Structural Analysis Applied to Epilepsy," in *Magnetic Resonance in Epilepsy*, R. Kuzniecky and G. D. Jackson, Eds. Burlington: Elsevier, 2005, pp. 249–269.
- [54] OpenCV, "Morphological Transformations-OpenCV," *OpenCV modules*, 2020. [Online]. Available: [https://docs.opencv.org/master/d9/d61/tutorial\\_py\\_morphological\\_ops.html](https://docs.opencv.org/master/d9/d61/tutorial_py_morphological_ops.html). [Accessed: Apr. 16, 2020]
- [55] S. N. Ashwindran, A. A. Azizuddin, and A. N. Oumer, "Study of  $\sqrt{2}$  Conjecture in the Construction of Drag Induced Wind Turbine Blade Morphology," *Evergreen*, vol. 8, no. 3, pp. 574–585, Sep. 2021, doi: 10.5109/4491649.
- [56] T. S. Rao, "Biofouling in Industrial Water Systems," in *Mineral Scales and Deposits*, Z. Amjad and K. D. Demadis, Eds. Amsterdam: Elsevier, 2015, pp. 123–140.
- [57] S. C. Dexter, "Marine and Natural Waters: Corrosion," in *Encyclopedia of Materials: Science and Technology*, K. J. Buschow, R. W. Cahn, and M. C. Flemings, Eds. Oxford: Elsevier, 2001, pp. 5172–5174.
- [58] R. De Nys and J. Guenther, "The impact and control of biofouling in marine finfish aquaculture," in *Advances in Marine Antifouling Coatings and Technologies*, C. Hellio and D. Yebra, Eds. Elsevier, 2009, pp. 177–221.
- [59] R. Hayashi et al., "Phylogenetic position and evolutionary history of the turtle and whale barnacles (Cirripedia: Balanomorpha: Coronoloidea)," *Mol. Phylogenet. Evol.*, vol. 67, no. 1, pp. 9–14, Apr. 2013, doi: 10.1016/j.ympev.2012.12.018.
- [60] H. Razaghian, B. S. Esfandabad, M. A. Hesni, R. V. Shoushtari, H. Toranjzar, and J. Miller, "Distribution patterns of epibiotic barnacles on the Hawksbill turtle, *Eretmochelys imbricata*, nesting in Iran," *Reg. Stud. Mar. Sci.*, vol. 27, p. 100527, Mar. 2019, doi: 10.1016/j.rsma.2019.100527.
- [61] T. Munk, D. Kane, and D. M. Yebra, "The effects of corrosion and fouling on the performance of ocean-going vessels: a naval architectural perspective," in *Advances in Marine Antifouling Coatings and Technologies*, C. Hellio and D. Yebra, Eds. Elsevier, 2009, pp. 148–176.
- [62] K. S. Jeon, J. I. Jeong, J.-K. Pan, and K.-W. Ryu, "Effects of end plates with various shapes and sizes on helical Savonius wind turbines," *Renew. Energy*, vol. 79, pp. 167–176, Jul. 2015, doi: 10.1016/j.renene.2014.11.035.
- [63] N. H. Mahmoud, A. A. El-Haroun, E. Wahba, and M. H. Nasef, "An experimental study on improvement of Savonius rotor performance," *Alexandria Eng. J.*, vol. 51, no. 1, pp. 19–25, Mar. 2012, doi: 10.1016/j.aej.2012.07.003.
- [64] T. Yuwono, G. Sakti, F. Nur Aulia, and A. Chandra Wijaya, "Improving the performance of Savonius wind turbine by installation of a circular cylinder upstream of returning turbine blade," *Alexandria Eng. J.*, vol. 59, no. 6, pp. 4923–4932, Dec. 2020, doi: 10.1016/j.aej.2020.09.009.
- [65] F. Bouak and J. Lemay, "Use of the wake of a small cylinder to Control unsteady loads on a circular cylinder," *J. Vis.*, vol. 4, no. 1, pp. 61–72, Mar. 2001, doi: 10.1007/BF03182456.